ISFV13 - 13th International Symposium on Flow Visualization
FLUVISU12 - 12th French Congress on Visualization in Fluid Mechanics
July 1-4, 2008, Nice, France

TOPOLOGY OF SUPERSONIC JET INTERACTION FLOWFIELDS AT HIGH PRESSURE RATIOS

Frank K. Lu*, Dean A. Dickmann,**
***University of Texas at Arlington, Arlington, Texas 76019, USA**
****Lockheed Martin Missiles and Fire Control, Grand Prairie, Texas 75265, USA**

KEYWORDS:
Main subject(s): *High Speed Flow, Computational Fluid Mechanics*
Fluid: *Aerodynamics*
Visualization method(s): *Computer Visualization, Skin Friction, Streamlines*
Other keywords: *Jet Interaction, Jet in Crossflow*

ABSTRACT: *The flow structure of a jet at high pressure issuing normally from an orifice in a flat plate into a supersonic stream was examined using a Reynolds-averaged Navier-Stokes solver. The study confirmed the presence of secondary horseshoe vortices as well as identified new vortical structures that emanated downstream of the jet.*

1 Introduction

The jet issuing normally from an orifice into a supersonic stream produces a complex three-dimensional flowfield, sometimes known as jet interaction (JI), which is rich in topological features. Some similarity exists between this flowfield and that induced by a cylindrical protuberance [1,2] that yields a so-called semi-infinite interaction [3], although the JI flowfield is further complicated by the interaction of two gas streams. The general near-field features of a JI are shown in Fig. 1 for a jet with a jet pressure ratio above unity [4]. The normal jet appears to be a blunt object to the incoming flow which produces a bow shock. This shock induces a three-dimensional, boundary layer interaction with a characteristic λ-foot shock structure and strong horseshoe vortices from vorticity creation via stretching of the vortex lines and baroclinic torque. The expanding jet is deflected by the main flow and a further shock, known as a barrel shock, is created. Vorticity creation within the jet produces a set of counter-rotating jet vortices which dominates the downstream flow. In addition, a reattachment shock is observed near the surface, downstream of the orifice.

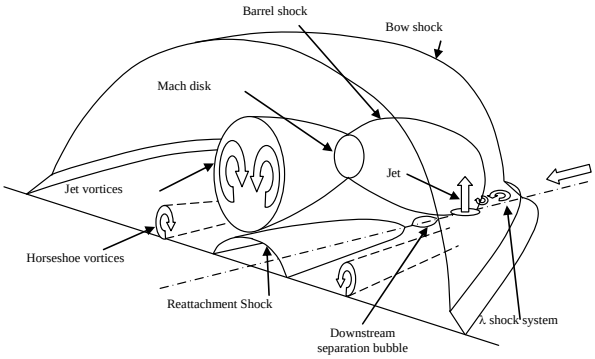

Figure 1. Currently accepted near field mean flow structure [4].

The flowfield structure described above is primarily obtained from experimental observations using shadowgraphy and laser lightscreen and was also guided by subsonic observations [5]. This flow continues to remain to be a topic of great interest, with recent studies utilizing nonintrusive flowfield mapping and large eddy simulations to provide extremely detailed

information. Technological interest in JI centers primarily on fuel injection into scramjet combustors [6–12] and in aerospace vehicle control [13–21].

This paper is concerned with topological features that arise at the high nozzle pressure ratios when JI is used for vehicle control purposes at high altitudes. It is well known that three-dimensional flows can possess a fascinating variety of topologies [22], the study of which dates to Poincaré in the late nineteenth century. For a long while, attention was placed primarily on surface topologies, particularly in high-speed aerodynamics, due to the difficulties of describing off-surface topologies in gaseous flows with its high level of diffusion or in the inherent unsteadiness at high Reynolds number. However, the ability to perform instantaneous or time-averaged flowfield mapping and computations have allowed detailed flowfield topologies to be revealed [23–26]. The present study reports new time-averaged features that observed through a parametric series of three-dimensional, Reynolds-averaged Navier-Stokes computations at various Mach numbers. There may be concern that flow unsteadiness, especially in the downstream region of the JI, may be important in understanding the physics of JI. Within the scope of this paper, this concern is obviously not addressed. However, the visualizations presented here provide details that hitherto have not been observed and thus represent a step toward a better understanding of the physics of JI.

2 Method

2.1 Governing Equations and Numerical Approach

The Reynolds-averaged conservation equations are solved numerically using a finite-volume scheme. The conservation equations are discretized using a first-order forward difference operator for the time derivative and a second-order central difference operator for the viscous terms. The Van Leer MUSCL upwind extrapolation is used for determining the face properties. Roe's flux splitting method is used for the inviscid flux terms. A two-equation κ-κl is used to model the turbulence [27]. The numerical model was validated against [28]. Further details, including a mesh refinement study and a discussion on convergence of the numerical solution, can be found in [29].

2.2 Configuration and Flow Conditions

The configuration comprised of a 457.2 mm square plate with a jet orifice, 2.54 mm in diameter, located on the centerline at 177.8 mm from the leading edge. The coordinate system is located at the center of the orifice, with x in the downstream axial direction, y in the normal direction and z in the spanwise direction. The orifice forms the exit of a convergent nozzle. The total pressure of the jet that leaves the nozzle is set by the pressure ratio. The results discussed are obtained at Mach 2, with others obtained at increments of Mach 0.5 to Mach 4.5, see Table 1. The total temperature for the freestream or jet is 244 K. Adiabatic conditions are assumed for the flat plate. The Reynolds number was set at 6.56 million per m for the entire study. To maintain a constant Reynolds number and total temperature requires that the pressure be varied, as is evident in Table 1. After the pressure is determined, the jet pressure ratio

$$PR = p_{tj} / p_{\infty} \tag{1}$$

which is the jet total pressure normalized by the freestream pressure, is also fixed at values ranging from 5 through 2000. Jet interactions at very high pressure ratios have not been

previously examined in detail and are of interest in the present study. Table 1 also lists the momentum flux ratio, defined as

$$J = \frac{\gamma_j p_j M_j^2}{\gamma_\infty p_\infty M_\infty^2} \tag{2}$$

Since the jet is air and the orifice is choked,

$$J = \left(1 + \frac{\gamma - 1}{2}\right)^{-\gamma/(\gamma-1)} \frac{PR}{M_\infty^2} \tag{3}$$

However, due to viscous effects that resulted in a vena contracta near the jet exit, the Mach number at the exit is not uniform and its average value is 1.15 for all the cases studied. This resulted in about a 15 percent underestimate in the value p_j and J. This underestimate is not significant for the present study which considers a wide range of J from 0.88 through 322. Finally, the flow is assumed to be turbulent from the leading edge. This assumption is not expected to result in errors in the JI phenomenon under investigation.

Table 1. JI cases examined.

M_∞	2.0						2.5	3.0	3.5	4.0	4.5
p_∞, kPa	9.85						7.87	6.56	5.62	4.92	4.38
PR	5	15	100	500	1000	2000	2000	2000	2000	2000	2000
J	0.88	2.64	17.6	87.9	176	322	206	143	105	80.5	63.6
V_j, m/s	303										

3 Results and Discussion

3.1 Surface Topology

To simplify the discussion, the skin friction topology will be examined first. The skin friction lines together with surface isobars for the cases examined at Mach 2 are shown in Fig. 2. Consider first the low PR = 5 case of Fig. 2a. The incoming surface flow encounters the obstacle posed by the normal jet and an open separation, labeled “global lines of separation” ensues [22]. Topological rules dictate the presence of a saddle point followed by an attachment node. Figures 2b–f show the same upstream surface topology but with the features spread further apart. The spread in the spanwise direction is larger than in the upstream direction.

While the upstream surface features appear to be the same but further spread out despite the large variation in jet pressure ratio, the downstream surface flow shows distinct changes mostly via a downstream stretching of the distances between the singularities. For the low PR = 5, three saddle points and a pair of foci of separation occur near the rear of the orifice. As the jet pressure ratio increases, the rear pair of saddle points is pushed further downstream and an attachment node is observed Note that the rear saddle point near the orifice remains fairly close to the orifice, but the other saddle point moves downstream and another saddle point along with an attachment node appear. A global line of separation in the downstream surface flow is also observed.

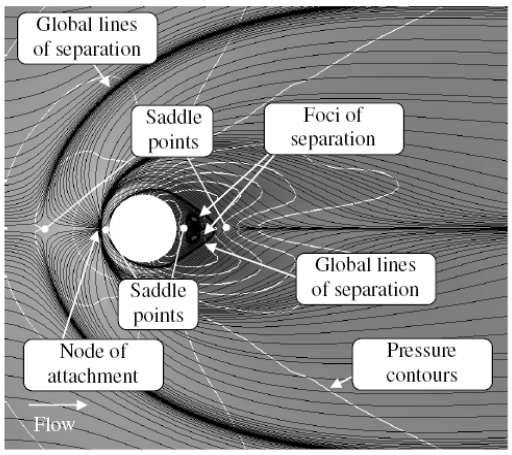

a. $PR = 5$.

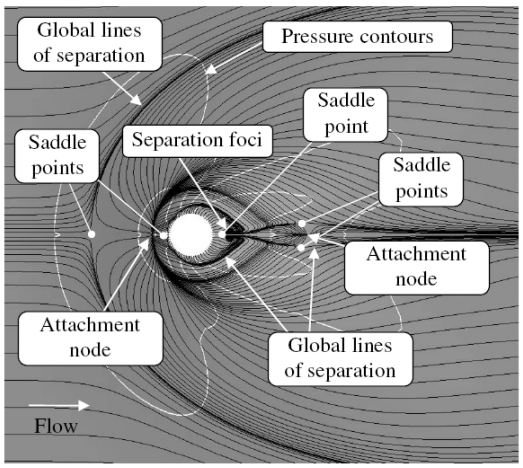

b. $PR = 15$.

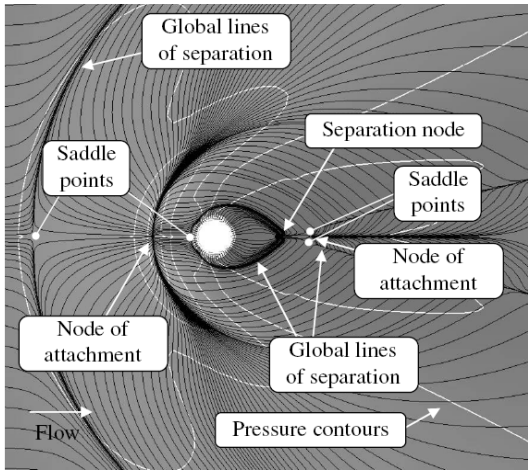

c. $PR = 100$.

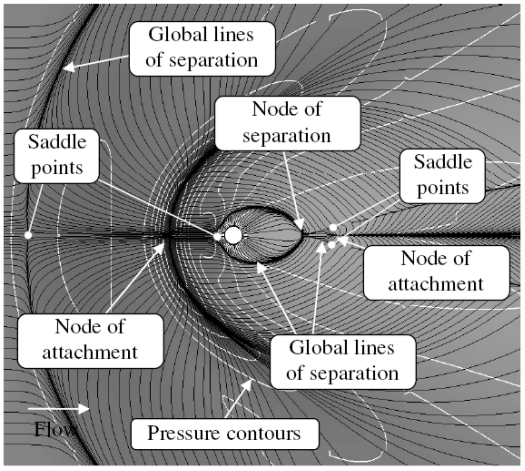

d. $PR = 500$.

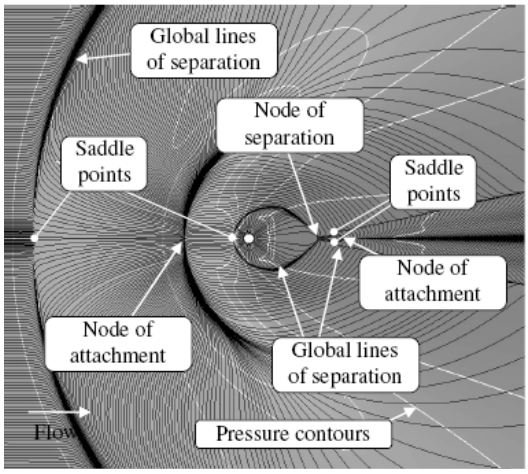

e. $PR = 1000$.

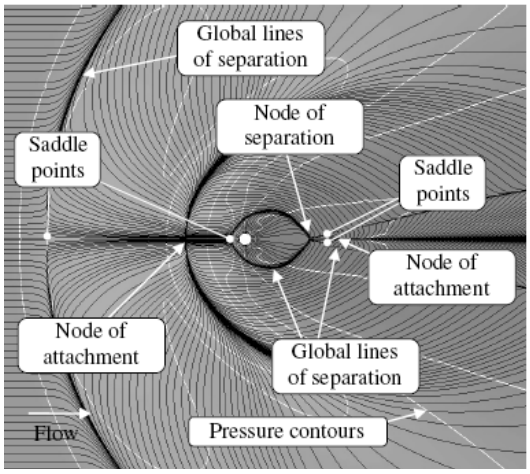

f. $PR = 2000$.

Fig. 2. Skin friction lines with surface isobars at Mach 2.

3.1 Flow Field Features

The surface topology does not fully reveal the complexity of the flow field, especially in the downstream region when the pressure ratio changes. For illustrative purposes, the salient flow field features for the Mach 2, *PR* = 15 case are shown in Fig. 3. Figure 3a shows an upstream λ-shock structure that arises from a shock/boundary layer separation. This separation results in a primary horseshoe vortex system that wraps itself around the jet which then trails downstream, as seen in Fig. 3b.[1] The primary horseshoe vortices are associated with the global line of separation. A small secondary vortex is also identified in Fig. 3a between the shock and the jet that had not been well identified by previous computations [10,19,20] although Roger and Chan [30] mentioned a characteristic double horseshoe vortex structure in front of the jet which proceeds around and downstream. Nonetheless, the present study shows that the secondary horseshoe vortices are blocked by the primary horseshoe vortices from the surface (Figs. 3b and c). This is thought to be why the secondary vortices are not captured by surface flow visualizations. Further, the secondary horseshoe vortex can become a significant feature when the PR is large.

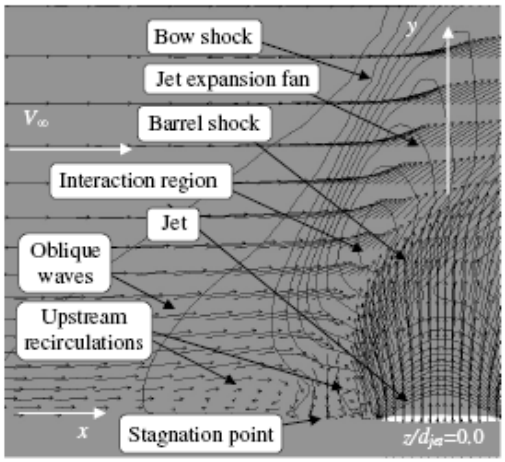

a. Isobars and velocity vectors in the upstream bisector plane.

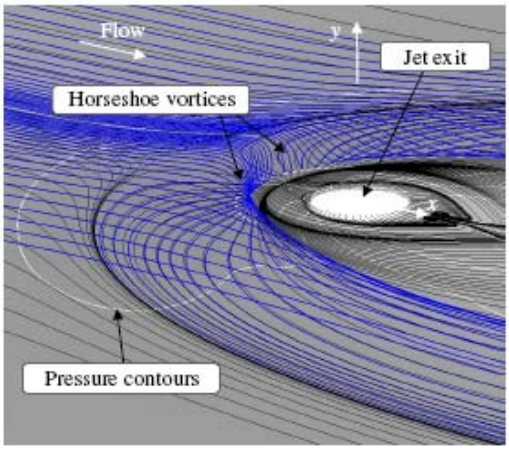

b. Primary horseshoe vortices from upstream flow separation.

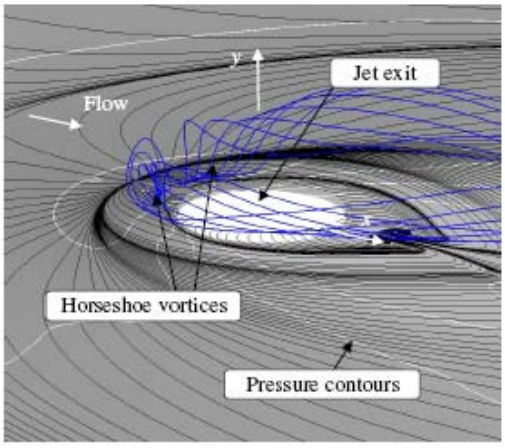

c. Secondary horseshoe vortices.

Fig. 3. JI upstream flowfield features at Mach 2, $PR = 15$.

[1]The primary horseshoe vortex is sometimes considered to be a pair of counter-rotating vortices, which is adopted presently.

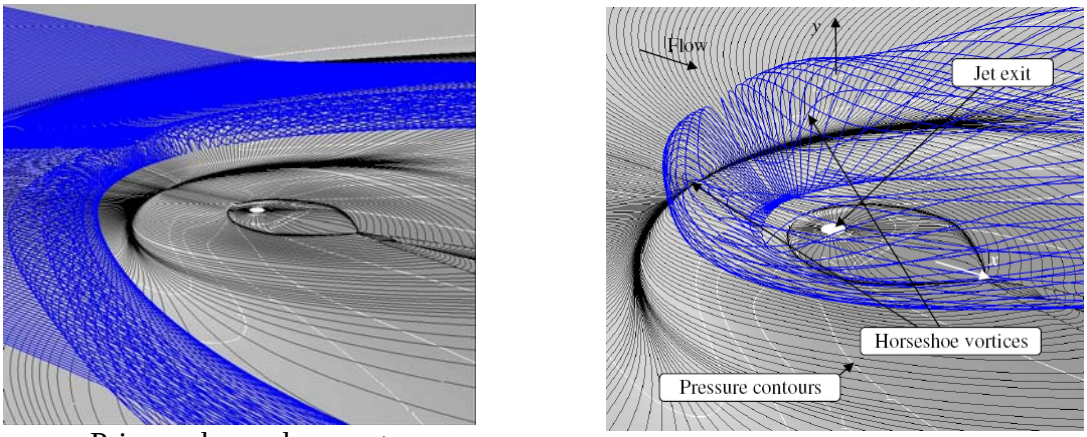

a. Primary horseshoe vortex. b. Secondary horseshoe vortex.

Fig. 4. Upstream horseshoe vortex for an incoming flow of Mach 2 and $PR = 2000$.

This is illustrated in Fig. 4 for PR = 2000, where the primary horseshoe vortex is shown in the left and the secondary horseshoe vortex is shown in the right. For a proper scale between the two subfigures, refer to the size of the jet orifice between them. It can be seen that the secondary vortex occupies a large vertical portion of the upstream interaction flowfield. The secondary horseshoe vortices also become more distinct with increasing jet pressure ratio, becoming a significant feature of the flowfield. This can be seen by a comparison between Figs. 3c and 4b for $PR = 15$ and 2000 respectively.

Downstream features are shown in Fig. 5. The jet vortices shown schematically in Fig. 1 are revealed in Fig. 5a. The simulations show that the jet and secondary vortices are intertwined, which may be why the secondary vortex was not previously revealed in experimental flow visualizations.

New downstream features are revealed in the present study. These include horn, near-field and far-field vortices, seen in Figs. 5b–d, respectively. The streamlines wrapping around the dividing surfaces emanating from the global separation lines formed into horn vortices which are small features just downstream of the orifice. These horn vortices are distinguished from the wake vortices, which have been reported in the past but not well understood either [14]. The present study shows that the wake vortices remain close to the surface and persists to the end of the computational domain.

4 Conclusions

Visualizations of time-averaged solutions of a jet issuing normally into a supersonic stream confirmed features that have been observed previously. In addition, the present study showed the existence of a secondary horseshoe vortex pair that intertwined itself with the jet vortices. The secondary horseshoe vortex pair remained within the flow and thus did not leave a footprint in surface visualizations. The study also revealed the presence of horn vortices just downstream of the orifice that were engulfed by the jet vortices. In addition, surface hugging wake vortices persist toward the exit of the computational domain.

References

1. Sedney, R. A survey of the effects of small protuberances on boundary-layer flows. *AIAA Journal*, Vol. 11, No. 6, pp. 782–792, 1973.

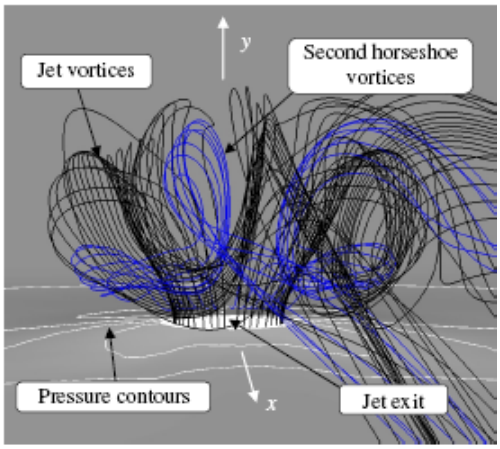

a. Jet vortices emanating from the orifice.

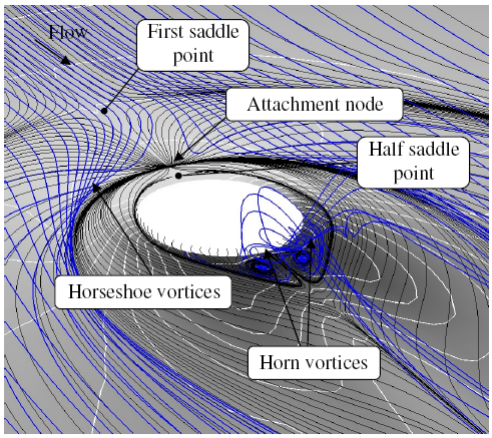

b. Horn vortices at the rear of the jet.

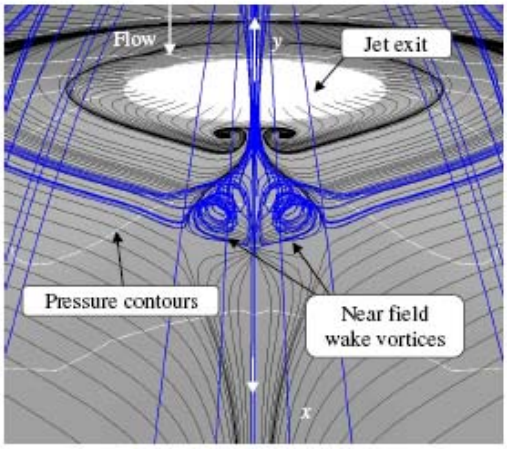

c. Near-field wake vortices.

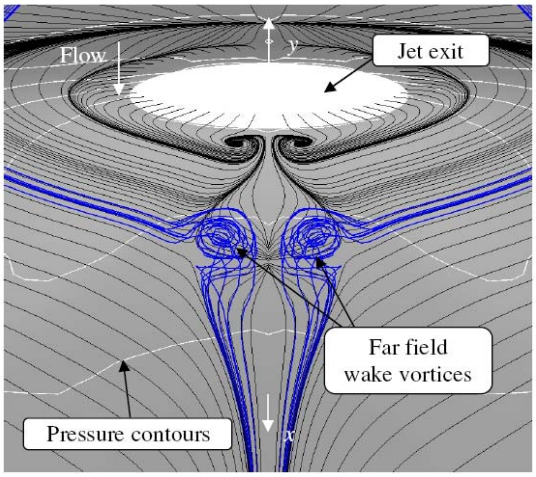

d. Far-field wake vortices.

Fig. 5. JI downstream flowfield features at Mach 2, $PR = 15$.

2. Sedney, R. and Kitchens, C.W., Jr. Separation ahead of protuberances in supersonic turbulent boundary layers. *AIAA Journal*, Vol. 15, No. 4, pp. 546–552, 1977.
3. Settles, G.S. and Dolling, D.S., "Swept Shock Wave-Boundary Layer Interactions," in *Tactical Missile Aerodynamics*, M. J. Hemsch and J. N. Nielsen (eds.), AIAA, 1986, pp. 297–379.
4. Champigny, P. and Lacau, R.G.. Lateral jet control for tactical missiles. Special Course on Missile Aerodynamics, AGARD-R-804, Paper No. 3, 1994.
5. Fric, T.F. and Roshko, A. Vortical structure in the wake of a transverse jet. *Journal of Fluid Mechanics*, Vol. 279, pp. 1–47, 1994.
6. Bogdanoff, D.W., "Advanced injection and mixing techniques for scramjet combustors," *Journal of Propulsion and Power*, Vol. 10, No. 2, pp. 183–190, 1994.
7. Belanger, J. and Hornung, H.G., "Transverse jet mixing and combustion experiments in hypervelocity flows," *Journal of Propulsion and Power*, Vol. 12, No. 1, pp. 186–192, 1996.
8. Gruber, M.R., Nejad, A.S., Chen, T.H., Dutton, J.C., "Bow shock/jet interaction in compressible transverse injection flowfields," *AIAA Journal*, Vol. 34, No. 10, pp. 2191–2193, 1996.
9. Santiago, J.G., and Dutton, J.C., "Velocity measurements of a jet injected into a supersonic crossflow," *Journal of Propulsion and Power*, Vol. 13, No. 2, pp. 264–273, 1997.
10. Sriram, A.T. and Mathew, J., "Numerical simulation of transverse injection of circular jets into turbulent supersonic streams," *Journal of Propulsion and Power*, Vol. 24, No. 1, pp. 45–54, 2008.

11. Byun, Y.H., Bae, K.J., Wallis, W., Viti, V., Schetz, J.A. and Bowersox, R., "Jet interaction in supersonic flow with a downstream surface ramp," *Journal of Spacecraft and Rockets*, Vol. 42, No. 1, pp. 38–44, 2005
12. Grossman, P.M., Maddalena, L. and Schetz, J.A., "Flush-wall, diamond-shaped fuel injector for high Mach number scramjets," *Journal of Propulsion and Power*, Vol. 24, No. 2, pp. 256–266, 2008.
13. Beresh, S.J. Heineck, J.T., Walker, S.M., Schairer, E.T. and Yaste, D.M., "Planar velocimetry of jet/fin interaction on a full-scale flight vehicle configuration," *AIAA Journal*, Vol. 45, No. 8, pp. 1827–1840, 2007.
14. Beresh, S.J. Henfling, J.F., Erven, R.J. and Spillers, R.W., "Vortex structure produced by a laterally inclined supersonic jet in transonic crossflow," *Journal of Propulsion and Power*, Vol. 23, No. 2, pp. 353–363, 2007.
15. Srivastava, B., "Computational analysis and validation for lateral jet controlled missiles," *Journal of Spacecraft and Rockets*, Vol. 34, No. 5, pp. 584–592, 1997.
16. Brandeis, J. and Gill, J., "Experimental investigation of super- and hypersonic jet interaction on missile configurations," *Journal of Spacecraft and Rockets*, Vol. 35, No. 3, pp. 296–302, 1998.
17. Graham, M.J. and Weinacht, P., "Numerical investigation of supersonic jet interaction for axisymmetric bodies," *Journal of Spacecraft and Rockets*, Vol. 37, No. 5, pp. 675–583, 2000.
18. Graham, M.J., Weinacht, P. and Brandeis, J., "Numerical investigation of supersonic jet interaction for finned bodies," *Journal of Spacecraft and Rockets*, Vol. 39, No. 2, pp. 376–383, 2002.
19. Cassel, L.A., "Applying jet interaction technology," *Journal of Spacecraft and Rockets*, Vol. 40, No. 4, pp. 523–537, 2003.
20. Min, B.Y., Lee, J.W. and Byun, Y.H., "Numerical investigation of the shock interaction effect on the lateral jet controlled missile," *Aerospace Science and Technology*, Vol. 10, No. 5, pp. 385–393, 2006.
21. Ebrahimi, H.B., "Numerical investigation of jet interaction in a supersonic freestream," *Journal of Spacecraft and Rockets*, Vol. 45, No. 1, pp. 95–103, 2008.
22. Tobak, M. and Peake, D.J., "Topology of three-dimensional separated flows," *Annual Review of Fluid Mechanics*, Vol. 14, pp. 61–85, 1982.
23. Foss, J.F. Surface selections and topological constraint evaluations for flow field analyses. *Experiments in Fluids*, Vol. 34, No. 6, pp. 883–898, 2004.
24. Brons, M., "Streamline topology: Patterns in fluid flows and their bifurcations," *Advances in Applied Mechanics*, Vol. 41, pp. 1–42, 2007.
25. Depardon, S., Lasserre, J.J., Brizzi, L.E. and Boreé, J., "Automated topology classification method for instantaneous velocity fields," *Experiments in Fluids*, Vol. 42, No. 5, pp. 697–710, 2007.
26. Surana, A, Jacobs, G.B. and Haller, G., "Extraction of separation and attachment surfaces from three-dimensional steady shear flows," *AIAA Journal*, Vol. 45, No. 6, pp. 1290–1302, 2007.
27. Smith, B.R., "The κ-κl turbulence model and wall layer model for compressible flows," AIAA Paper 90–1483, 1990.
28. Dowdy, M.W. and Newton, J.F., "Investigation of liquid and gaseous secondary injection phenomena on a flat plate with M =2.01 to M = 4.54," JPL TR 32-542, December 23, 1963.
29. Dickmann, D.A., "On the near field mean flow structure of transverse jets issuing into a supersonic freestream," Ph.D. dissertation, University of Texas at Arlington, December 2007.
30. Roger, R.P. and Chan, S.C., "CFD study of the flowfield due to a supersonic jet exiting into a hypersonic stream from a conical surface II," AIAA Paper 93-2926, 1993.

Copyright Statement